


 CrossMark
click for updates

Cite this: DOI: 10.1039/c6sm01692h

Thermoosmotic microfluidics

 Mingcheng Yang^{*a} and Marisol Ripoll^{*b}

 Received 24th July 2016,
Accepted 12th September 2016

DOI: 10.1039/c6sm01692h

www.rsc.org/softmatter

Microchannels with asymmetrically ratcheted walls are here shown to behave as effective and versatile microfluidic pumps if locally heated. When the boundary walls have different temperatures, the confined liquid experiences a temperature gradient along the sawtooth edges, which can induce a thermoosmotic flow. A mesoscale molecular simulation approach is here employed to investigate the flows which are contrasted using an analytical approach. Microchannels can be composed by one or two ratcheted walls which can be straight or cylindrical. Varying the channel geometry can not only change the overall fluid flux, but also vary the flow patterns from shear to capillary type, or even to extensional type flows. This scheme does not require multiphase fluids or any movable channel parts, although they are possible to be implemented. The proposed principle is then very versatile to locally manipulate complex fluids, and a promising tool to recover waste heat, to facilitate cooling of microchips, and to manufacture portable lab-on-a-chip devices.

1. Introduction

Microfluidics has attracted great attention during the last two decades due to its unique advantages in applications of chemistry, biology, or medicine.¹ Microfluidic devices in general, and lab-on-a-chip devices in particular, completely rely on the capacity of generating and controlling fluid flows at the micro- or nanometer scale.² Generally, flows are generated by external forces that can be done mechanically, or by imposing a pressure difference between the inlet and the outlet flows.^{2–4} Such driving mechanisms become increasingly less efficient with miniaturization because of the huge increase in hydrodynamic resistance that comes with downsizing. Furthermore, both options rely on external mechanisms that importantly hamper the portability of the devices.¹ An alternative is to induce stresses localized at the boundaries, which is particularly effective on a small scale due to a large surface to volume ratio. Nature has solved this issue with microscopic ciliated systems. These systems are able to generate flows with different motion patterns,^{5,6} and are of fundamental importance in various physiological processes such as embryo development,⁷ and in the self-propulsion of microorganisms such as *Paramecium*.⁸ Various artificial routes used until now to induce boundary stresses mimic nature by constructing artificial cilia which are actuated by external electric or magnetic fields.^{9,10}

An attractive strategy to induce both flow and particle self-propelled motion has been found in phoretic mechanisms.^{11–17}

Phoresis refers to the directed motion induced to a suspended particle due to an inhomogeneous surrounding, which can be, for example, a temperature gradient (thermophoresis), a concentration gradient (diffusiophoresis) or an electric potential gradient (electrophoresis). Conversely, as a consequence of Newton's third law, the gradient fields can generate the motion of a fluid at a fixed solid–fluid interface, which is usually referred to as phoretic osmosis, and in the case of a fluid–fluid interface, which is known as phoretic capillary. In contrast to the flows produced by chemical gradients, or the widely used electric field, thermal gradient-driven motion works equally well in charged and neutral solutions, being pollution-free due to the absence of surfactants or chemical fuels. Furthermore, thermal gradient-driven motion allows optical microscale operations with optical heating which is the basis of the emerging field of optofluidics.^{18,19}

The applications of thermocapillary and thermoosmosis in microfluidics have been severely limited due to the proportionality of the flow velocities to the temperature gradients. Very large temperature differences are then required at the two ends of the microchannel. Two avenues have been suggested to surmount this problem. The first one uses a symmetric temperature gradient along a composite channel, with a heterogeneous wall composition²⁰ or with heterogeneous heating.²¹ The inhomogeneous boundary–liquid interactions lead then to a net flow. The second strategy considers a temperature gradient normal to the channel substrate that presents a pattern of asymmetrical grooves, in which Marangoni–Bénard convection together with the asymmetric topographical pattern act as a ‘fluidic ratchet’ to cause a global flow in the transverse direction.²² Compared with the first strategy, the fluidic ratchet only needs homogeneous boundary walls, and facilitates the generation of large temperature gradients

^a Beijing National Laboratory for Condensed Matter Physics and Key Laboratory of Soft Matter Physics, Institute of Physics, Chinese Academy of Sciences, Beijing 100190, China. E-mail: mcyang@iphy.ac.cn

^b Theoretical Soft-Matter and Biophysics, Institute of Complex Systems, Forschungszentrum Jülich, 52425 Jülich, Germany. E-mail: m.ripoll@fz-juelich.de

because of extreme confinement and performance of thermal management owing to an easy connection with the heat source. The fluidic ratchet however requires the existence of a deformable interface between two immiscible fluids, where Marangoni–Bénard convection is triggered. Different approaches are therefore needed to pump single-phase liquids confined in solid channels, as encountered in most microfluidic devices.

A promising alternative mechanism has been recently proved in asymmetric ratcheted structures. An asymmetric gear with homogeneous surface properties has been proposed to fabricate thermo- or diffusiophoretic microrotors.^{23,24} Gears can be heated in a cool surrounding fluid, or catalyze chemical reactions at their surface. The resulting temperature or concentration gradients along the gear teeth produce a directed phoretic force, which leads to a net torque on the gear and consequently its spontaneous unidirectional rotation. Recent experimental results have confirmed this extent for a heated homogeneous gear at a liquid–air interface.²⁵ An analytical approach has explored a diffusi-osmotic pump, and investigated how the induced flux of a straight channel with one ratcheted wall depends on the chemical properties and shape of the ratcheting teeth.^{26,27}

Inspired by the previous mechanisms, here we propose various thermal-driven fluidic ratchets. These are microchannels composed by one or two walls with an asymmetric sawtooth pattern with a straight or a cylindrical configuration. When the boundary walls are maintained at different temperatures, the confined liquid will display a primary temperature gradient perpendicular to the channel, and a secondary one along the sawtooth edges. The related thermoosmosis originating from the secondary temperature gradient can then induce a net flow parallel to the channel. This mechanism does not rely on a deformation free interface, such that it can be employed in single-phased liquids. On the other hand, multiphase systems, or the presence of deformable interfaces will also generate thermocapillary which would eventually enhance the flow. Mesoscale molecular simulations are performed to investigate the flow in single-phase liquids, which can be compared with analytical predictions. Different channel geometries are shown to increase or decrease the related flux, and more importantly modify it from shear to capillary-type flow, and interestingly also to extensional flow. The proposed thermal pump provides a simple and effective manner to manipulate liquids without the necessity of any movable part, or external coupled devices, and where the flow can be locally switched on and off by local application of heat as provided by a laser.

II. Simulation model and method

In response to the temperature gradient, a suspended particle experiences a thermophoretic force, \mathbf{f}_T .^{28–30} This force arises from the interactions of the particle with the surrounding non-isothermal solvent being directly proportional to the temperature gradient, ∇T . Furthermore, \mathbf{f}_T strongly depends on the material properties such that

$$\mathbf{f}_T = -\alpha_T k_B \nabla T, \quad (1)$$

with α_T being the thermal diffusion factor, a dimensionless material constant. By convention, α_T is positive for thermophobic materials and negative for thermophilic ones. The nature of the particle–fluid interactions determines the value of α_T which changes not only with composition, but also with other factors such as average temperature and density.^{28,31–33} Equivalently, the thermophoretic force can also be understood as the result of the variation in liquid–solid surface tension induced by the inhomogeneous temperature. This force results in the drift of movable particles (thermophoresis), and in the long-ranged motion of the surrounding fluid for fixed objects (thermo-osmosis).^{11,21,31,34–36}

A hybrid two-dimensional simulation scheme is employed to model the microfluidic pumps. The fluid is described by a particle-based mesoscopic method known as multiparticle collision (MPC) dynamics,^{37–40} while the channel and its interactions with the fluid are simulated by molecular dynamics (MD) simulations. This hybrid dynamics scheme is very efficient and simultaneously satisfies all essential physics required to investigate these devices, such as hydrodynamic behavior, thermal fluctuations, heat conduction, and sustainability of temperature inhomogeneities.

MPC fluid

In MPC, the fluid is modelled by a collection of point-like particles of mass m . The particle dynamics takes place by alternating streaming and collision steps. In the streaming step, the fluid particles move ballistically for a certain time h . In the collision step, the particles are sorted into square cells of size a , and interchange momentum relative to the center-of-mass velocity of each collision cell. Although the solvent angular momentum conservation has not shown any influence on thermoosmotic flows,⁴¹ we use the stochastic rotation collision rule with variable collision angle introduced by Ryder and Yeomans,^{42,43} which ensures angular momentum conservation. Simulation units are reduced by setting $a = 1$, $m = 1$, and $k_B \tilde{T} = 1$ with k_B being the Boltzmann constant and \tilde{T} a reference temperature, such that, for example, velocities are measured in units of $\sqrt{k_B \tilde{T}/m}$. Mapping to experimental units can be performed by comparing the characteristic parameters of the simulations and the experimental system, as discussed at the end of the paper. Other employed MPC parameters are $h = 0.1$ and the mean number of fluid particles per cell $\rho = 12$. The viscosity of the MPC fluid with these parameters is measured as $\eta \simeq 9.2$, and using the existing kinetic theory for MPC with a stochastic rotation of a fixed angle,⁴⁴ we can estimate that the fluid has a Schmidt number $Sc = 13$, which corresponds to a liquid-like behavior.

Microchannel walls

The channel and its interactions with the fluid are simulated by molecular dynamics (MD) simulations. Walls are constructed by mounting a single layer of beads along the desired profile (planar, circular, ratcheted or straight) using harmonic springs

of constant $k = 600k_B\tilde{T}/a^2$. Here, the equilibrium position of each bead is exactly located at the wall profile, and the separation between neighboring beads is a , with no further interactions between different beads. The space between the walls is filled with the MPC fluid, and the interaction between wall beads and MPC particles is determined *via* MD simulations with Lennard-Jones (LJ) type potentials^{45,46} $U_k(r) = 4\epsilon \left[\left(\frac{\sigma}{r}\right)^{2n} - \left(\frac{\sigma}{r}\right)^n \right] + c$ for $r \leq r_c$. Here r is the distance between the bead center and the fluid particles, ϵ refers to the potential intensity, σ to the bead radius, and n is a positive integer describing the potential stiffness. The attractive and repulsive LJ potentials are obtained by considering $c = 0$ and $c = \epsilon$, respectively, together with the corresponding cutoff distance r_c . The bead radius is taken as $\sigma = 1.25a$, and $\epsilon = k_B\tilde{T}$. An efficient energy exchange between the wall beads and the MPC particles is obtained by considering the bead mass $M = m$. Note that the large overlap between neighboring beads prevents the fluid MPC particles from penetrating into the walls. The equations of motion of the beads and the interacting fluid are integrated with a velocity-Verlet MD algorithm. Various simulations are performed with just one structural unit repeated by periodic boundary conditions. Some simulations are performed with two or with four repeated structural units, together with transversal periodic boundary conditions. The results are shown to be independent of the number of repeated units, besides statistical precision, such that we do not make a precise distinction in this respect. It is important to emphasize that the choice of LJ potential constitutes a coarse-grained description of the interactions at the wall surface and will critically influence the value of α_T . This means that relevant specific details such as the frequently determinant system charges are taken into account only in the value of the thermal diffusion factor α_T , which determines the flow magnitude and direction.

Temperature inhomogeneity

To generate a temperature difference between the two walls, we apply an Andersen thermostat⁴⁷ to every wall bead. The velocity of each bead is therefore independently extracted from a Maxwellian distribution of a fixed temperature every ten MD steps. The temperature for all the beads at the cold wall is T_c , while for the beads at the hot wall the fixed temperature is $T_h = T_c + \Delta T_0$. Since the MPC fluid is in contact with the wall beads, it reaches, after a short relaxation time, a steady-state temperature distribution.⁴⁸ The strength of the thermophoretic effect is known to increase with the softness of the potential,⁴⁶ such that our simulations consider mostly very soft repulsive Lennard-Jones potentials ($n = 3$) for the sawtooth wall-fluid interactions, and also attractive interactions. In this way, both thermophilic and thermophobic forces are respectively taken into account.⁴⁶ The interactions with planar walls do not qualitatively determine the flow, such that a hard repulsive potential ($n = 24$) is used for the bead-fluid interactions, which minimizes the temperature jump at the wall, and therefore maximizes the temperature gradient.

III. Simulation results

Five microchannel geometries with five associated flow field types are now discussed. The investigated microchannels have at least one wall with a ratcheted profile; with the exception of the symmetric case, the short ratchet edges are perpendicular to the channel direction. The induced flow is therefore directly related to the temperature gradient tangential to the long ratchet edge ∇T_{\parallel} . The sawtooth wall-fluid interactions are both repulsive and attractive Lennard-Jones potentials, such that both thermophobic and thermophilic forces are respectively taken into account.⁴⁶ Although most simulations are performed in two dimensions, we have verified in the single ratcheted pump geometry that three-dimensional simulations lead to essentially the same results.

Single ratcheted pump: shear-like flow

A single-phase liquid confined by a cold flat wall and a hot sawtooth-shaped wall according to Fig. 1a is considered. The walls have a parallel orientation and are separated by a distance H . The ratcheted wall has sawteeth of height W separated by a distance D . The slope of each sawtooth is then given by an angle θ with $\sin \theta = D/(D^2 + W^2)^{1/2}$. The simulation channel has dimensions $D = 31$, $W = 8$ and $H = 20$, and $\Delta T_0 = 1.0$ is the externally imposed temperature difference (with $T_h = 1.5$ and $T_c = 0.5$). These are the reference values used in our simulations, which are fixed unless otherwise stated. These units refer to simulation values which can be related to experimental units as it will be discussed in section IV. The constituent beads of the sawtooth wall interact with the fluid particles *via* a soft repulsive LJ potential. Such a single bead in an external temperature gradient, interacting with this potential is characterized by $\alpha_T^b = -1.0$.⁴⁹ The effective thermal factor of the wall per unit length α_T is therefore expected to be directly proportional, and of the same order of magnitude, to this value $\alpha_T \propto \alpha_T^b$, and to display thermophilic properties.

After the system has reached the stationary state, we measure the temperature and the velocity fields of the liquid within the microchannel, as plotted respectively in Fig. 1b and c. The thermophilic properties of the ratcheted wall induce a flow that goes from the warmer to the cooler regions. Given the chosen geometry, this explains the overall flow from right to left and the counter-clockwise vortexes close to each short edge of the sawtooth wall in Fig. 1c.

The velocity profiles in four axes along the channel are displayed in Fig. 1d. In the central axes, far from the short ratchet edges, the flow is of the shear-type with the fluid velocity maximum nearest to the sawtooth wall, and close to vanishing in the proximity of the flat wall. This is because the sawtooth wall is the driving boundary while the flat wall only contributes to some hydrodynamic friction. The boundary axis at the narrowest channel point shows a lower velocity close to the walls increasing towards the center. The small velocity at the walls is due to the vanishing temperature gradients both at the ratchet tip and the flat wall. The larger central velocity is due to the continuity of the induced flux along the channel.

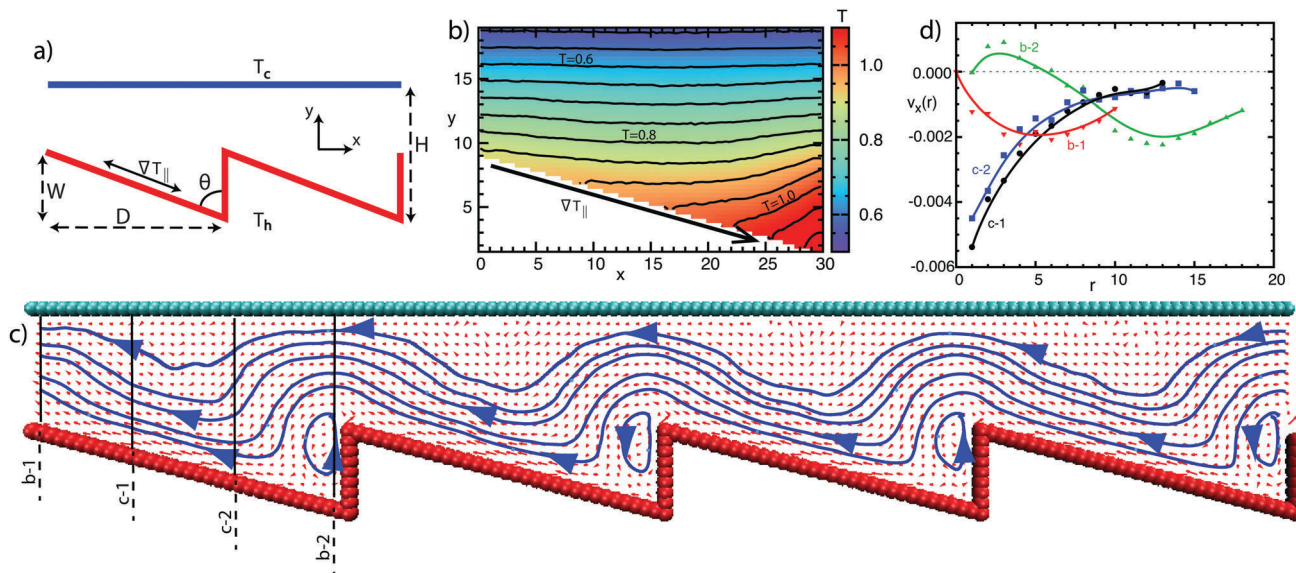


Fig. 1 (a) Schematic diagram of a thermoosmotic asymmetrically single ratcheted pump. When the sawtooth-shaped wall has a higher temperature than the flat wall ($\Delta T_0 > 0$), ∇T_{\parallel} points to the cleft of the sawtooth, otherwise to the summit of the sawtooth. (b) Temperature distribution of the fluid confined in a single ratcheted channel. The straight wall has a fixed temperature $T_c = 0.5$, while the ratcheted wall has $T_h = 1.5$. Isothermal lines are shown in black. (c) Streamlines (blue lines) and flow velocity (red arrows) for a thermoosmotic single ratcheted microchannel. (d) Flow velocities in the channel direction in the axis indicated in (c), as a function of the distance from the hot wall.

The boundary axis at the widest channel point shows a non-monotonous behavior due to the gradient of temperature along the short ratchet edge.

Induced flux

The flux induced by this microfluidic pump can be not only directly measured in the simulations, but also quantitatively characterized by the channel dimensions and the thermoosmotic properties of the wall and the fluid. The fluid in the vicinity of the large sawtooth edge is accelerated by the thermoosmotic driving force, *i.e.*, the reaction force of the thermophoretic force experienced by the wall. The fluid velocity increases until the corresponding hydrodynamic friction exactly counterbalances the driving force. From eqn (1), the steady-state flow velocity at the sawtooth surface \mathbf{v} then follows

$$\mathbf{v} = \frac{1}{\gamma} \alpha_T k_B \nabla T_{\parallel}. \quad (2)$$

Here, γ refers to the effective frictional coefficient per unit length of the microchannel, which together with α_T are fluid-wall properties. The fluid velocity along the channel can then be approximated by $u = \sin \theta |\mathbf{v}|$, and the flux through an effective channel of cross section $(H - W)$ by

$$j \sim \rho u (H - W) \simeq \rho \frac{\alpha_T}{\gamma} k_B \nabla T_{\parallel} \frac{D(H - W)}{(D^2 + W^2)^{1/2}}. \quad (3)$$

Given that the heat flux is mainly directed normal to the channel orientation, it is reasonable to assume that the liquid temperature changes linearly in this direction. Fig. 1b shows that, not being exact, this is a reasonable approximation. Thus, the temperature difference ΔT between the cleft area and the

summit area of each sawtooth is

$$\Delta T \sim \Delta T_0 \frac{W}{H}. \quad (4)$$

Therefore, the mean temperature gradient along the long edge of the sawtooth wall reads

$$|\nabla T_{\parallel}| \sim \Delta T_0 \frac{W}{H(D^2 + W^2)^{1/2}}. \quad (5)$$

However, this approximation should be taken carefully, due to at least two reasons. As can be seen in Fig. 1b, the modification of the temperature field is intrinsically different around the cleft and summit areas, and this is not taken into account in eqn (5). On the other hand, it should be noted that eqn (5) predicts a finite ∇T_{\parallel} for vanishing W if W/H is fixed and a constant ∇T_{\parallel} for vanishing W with both θ and H being fixed. With these considerations, the fluid flux can be approximated employing eqn (5) as

$$j \sim \rho \frac{\alpha_T}{\gamma} \Delta T_0 \frac{DW(H - W)}{H(D^2 + W^2)}. \quad (6)$$

To compare with the previous approximation, simulations are performed to compute the fluid flux pumped by the microchannel. We sequentially vary all system parameters, leaving the other ones fixed to the reference values. For a straightforward comparison, eqn (6) is plotted in Fig. 2 using the relation $\gamma = \eta/A$ with A being a unique fit parameter. The results are displayed in Fig. 2 and the dependence can be understood from the approximation in eqn (6) as follows:

(a) In Fig. 2a the net flux shows a maximum with varying sawtooth width D . Eqn (6) predicts a maximum around $D = W$,

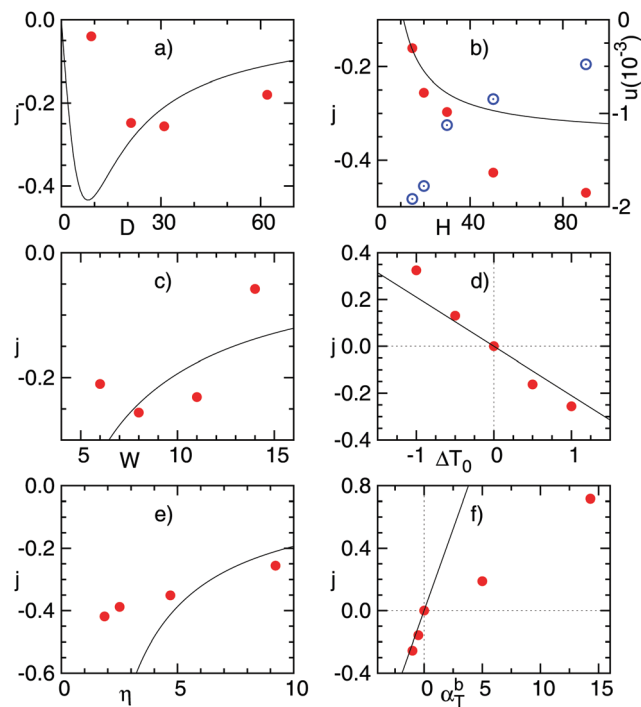


Fig. 2 Net fluid flux pumped along the microchannel as a function of the system parameters; (a) dependence on the sawtooth width D ; (b) on the channel height H ; (c) on the sawtooth height W by fixing $\theta \approx 75^\circ$ ($D/W \approx 3.8$); (d) on temperature difference ΔT_0 ; (e) on the fluid viscosity η (hence γ); (f) on the thermal diffusion factor of sawtooth beads α_T^b . Red solid circles correspond to the net flux j . Blue open circles in (b) refer to the mean transverse flow speed u . Lines correspond to eqn (6) with a single fit prefactor $A = 1.11$.

which in our simulation results appears at considerably larger D values.

(b) The pumped flux in Fig. 2b shows to monotonously increase with H , agreeing with the prediction in eqn (6). On the other hand, the mean net flow speed, $u \sim j/(H - W) \sim 1/H$, is expected to monotonously decrease with H , as also reproduced in Fig. 2b.

(c) The sawtooth height W is varied by keeping the angle θ ($\tan \theta = D/W$) unchanged, such that the shape of the sawtooth remains unvaried. The resulting pumped flux in Fig. 2c shows a maximum with respect to W , which is not predicted by eqn (6) for this case. This difference is due to the approximation in eqn (5) since a vanishing ∇T_{\parallel} for W approaching zero would imply a maximum value of the flux.

(d) The pumped flow across the channel has a clear linear dependence on the temperature difference between the walls ΔT_0 as depicted in Fig. 2d and predicted in eqn (6). This implies that the flow is simply reversed when warm and cold walls are interchanged.

(e) Varying the MPC fluid properties like the collision interval h and the average particle number ρ is known to change the fluid viscosity η .^{38,50,51} On the other hand, the fluid viscosity is expected to be directly proportional to the hydrodynamic friction coefficient γ , and hardly influences the thermoosmotic driving force. The monotonic decrease of the flow with

η observed in Fig. 2e therefore agrees with the behavior expected from eqn (6).

(f) Changing the bead-MPC fluid interactions changes the bead thermal factor α_T^b , and consequently the overall wall thermal factor α_T . We have employed repulsive LJ potentials with $n = 3$ and 6 which correspond to a thermophilic behavior with $\alpha_T^b = -1.0$ and -0.5 , respectively. Thermophobic attractive LJ potentials with $n = 12$ and 6 and $\alpha_T^b = 5.0$ and 14.3 , respectively are also used. The results in Fig. 2f display a monotonous increase as expected from eqn (6). The linear dependence seems though to have a different slope for the thermophobic and the thermophilic interactions. This can be related to the fact that increasing attraction also increases the stickiness of the boundary wall, which enhances the effective friction coefficient γ . Therefore, the slope of the flux j with α_T^b curve is smaller for positive values than for negative values of α_T^b .

Despite the employed rough approximation, the expression for the pumped flux in eqn (6) succeeds in qualitatively explaining the obtained simulation results, besides the dependence on the sawtooth height as discussed in Fig. 2c. This convincingly proves that the present fluidic ratchet indeed results from thermoosmosis due to the geometry-induced tangential thermal gradient. The qualitative agreement also suggests that the pumping capability of the thermoosmotic fluidic ratchet can be flexibly tuned by several different control parameters.

We finally point out that Knudsen-type pumps with similar ratchet structures have recently been proposed to induce fluxes of rarefied gases with applied temperature differences.^{52–54} The driving mechanism in these pumps is the so-called thermal creep, which refers to the flow induced in a rarefied gas interacting with a wall with a temperature gradient. The cooler gas particles are simply reflected to cool areas and the warmer to the warm areas biasing the gas probability distribution function. This generates a flow that goes always from cold to warm areas, and that does not depend on the nature of the gas-wall interactions. Thermal creep is therefore fundamentally different from the liquid thermoosmosis considered in our work.

Double ratcheted channel: inverted capillary flow

The previous microchannel can be modified by considering two parallel ratcheted structures, as depicted in Fig. 3a. Corresponding to a microchannel manufactured with a single material, we simulate all the wall beads with the same bead-fluid potential interactions. Driving forces of equal direction originate in both confronted walls. In the example depicted in Fig. 3a we choose $H = 28$, such that the channel dimensions are comparable to the reference values of the previous section. The resulting temperature gradients at the long edges of the ratcheted walls are smaller than that in the single ratcheted channel and the total flux is measured to be 33% larger. This value of the flux can be explained as the linear superposition of the flux induced independently by each wall in terms of its actual temperature gradient.

But the differences between the single and the double ratcheted micropumps are not only quantitative. The flow profiles along the channel are also different. The velocity profiles in four

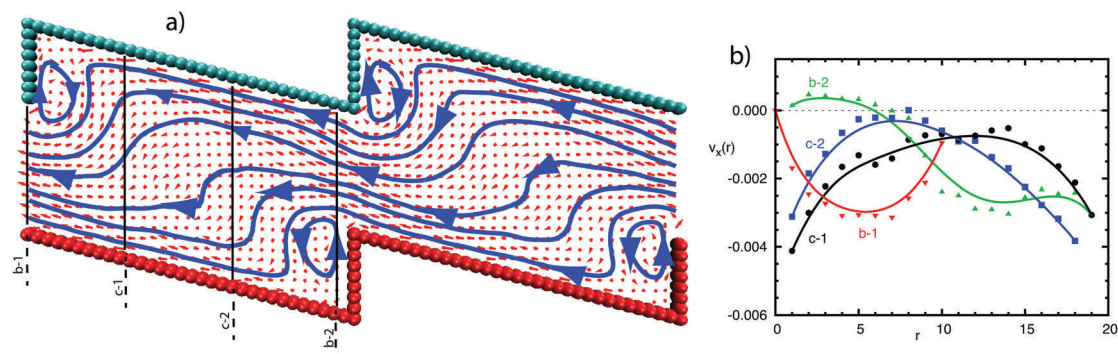


Fig. 3 (a) Flow field and streamlines generated by a microchannel with two ratcheted thermophilic parallel walls. (b) Flow velocities in the channel direction in the axis indicated in (a) as a function of the distance from the hot wall.

axes along the channel are displayed in Fig. 3b and can be compared to those in Fig. 1d. In the boundary axes, close to the short ratchet edges, the velocity is similar in both geometries. Nevertheless in the central axes, far from the short ratchet edges, the flow is of the inverted capillary type. The thermoosmotic driving forces are present in both walls such that the fluid velocity is maximum nearest the sawtooth walls, and almost vanishing in the center of the channel, producing a roughly parabolic profile. These different profiles are relevant, for example, in the case that there are suspended particles in the fluid. These particles will have very different adsorption or accumulation properties in the two geometries leading to a different overall behavior.

Specularly ratcheted channel: elongational flow

In the case that the two ratcheted walls do not have the same orientation but are specularly oriented, the induced flow differs significantly, as can be seen in Fig. 4a. The thermoosmotic driving forces have opposite signs in the two walls, such that in

this case the net flux will mostly vanish. A small flux can appear as a consequence of the temperature dependence of the wall thermophoretic properties. Besides this, a shear profile could be expected, although this is modified by the device geometry as can be seen in Fig. 4a. Close to the small ratchet edges, in the center of the channel (crossing of the axes *a-1* and *b-2*) the flow is consistent with the confluence of four counter-rotating vortices, as is typical for elongational flow. The elongation flow is confirmed by the velocity profiles in Fig. 4b. The velocity along the channel direction $v_x(r)$ close to the central horizontal axis varies linearly with the distance from the wall in the four tested axes. Simultaneously, the velocity perpendicular to the channel $v_y(r)$ in the axis parallel to the channel direction (*a-1*) has the same linear variation. This allows us to characterize the flow as elongational. A device based on a specularly ratcheted channel can therefore be useful for measuring elongational viscosity. Such devices have been built based on movable walls or confluence of an inlet and outlet crossing flows, in contrast to the device that we propose here.

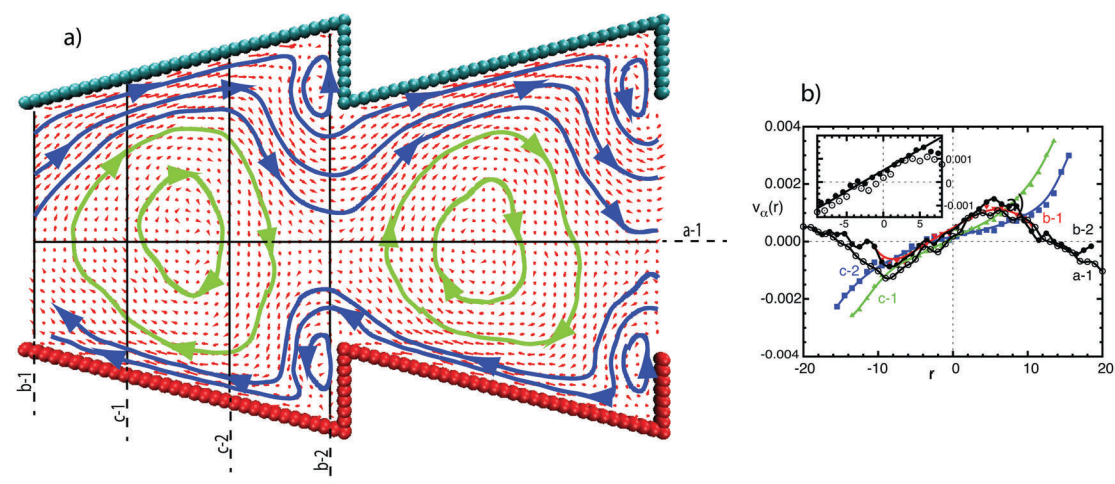


Fig. 4 (a) Flow field and streamlines generated by a microchannel with two ratcheted thermophilic walls with a specular orientation. Counter-rotating flow in the channel center is highlighted with a different colored streamline. (b) Flow velocities in the axes indicated in (a) as a function of the distance from the channel central axis. Closed symbols correspond to the velocity along the channel $v_x(r)$, for the four axes perpendicular to the main channel direction. Open symbols account for the velocity perpendicular to the channel direction $v_y(r)$ for the central axis *a-1* along the channel. The inset is a zoom-in of the fluid velocity in the center of the channel, where the flow is purely elongational.

On the other hand, the geometry proposed here is very similar to that of the fluidic rectifiers,⁵⁵ although the underlying physics and system behavior are completely different. The rectifiers account for the fact that a viscoelastic fluid has a flow resistance significantly different in back and forth directions.

Symmetrically ratcheted channel: Rayleigh–Bénard convection-like flow

A microchannel with one flat wall and one with a symmetric sawtooth profile, as displayed in Fig. 5, is now discussed. In this case, the sawtooth edges generate the thermoosmotic flows due to the presence of non-zero tangential temperature gradients. The thermoosmotic flows induced in the two edges of each tooth are symmetric with respect to the longitudinal symmetric axis of the channel, such that no net flux along the channel is produced. On the other hand, it is very interesting to observe in Fig. 5 that this geometrical structure generates fluid counter rotating vortexes similar to those in Rayleigh–Bénard convection.⁵⁶ Rayleigh–Bénard convection appears in plane horizontal layers of the fluid heated from below, namely with gravity acting in the same direction as the temperature gradient. In spite of the similarities between the two flows, they are fundamentally different. The thermoosmotic flow we propose here does not correspond to the instability of the fluid, such that the flow can increase continuously from zero by increasing the temperature difference (see a similar effect in Fig. 2d). This means that there is no critical threshold to trigger the fluid flow, such as the Rayleigh number in the buoyancy-driven flow. Furthermore, the geometry considered in our work can be regarded as microgravity, since gravity is simply not taken into account in our simulations. The angular velocity of these vortexes will depend on all system parameters in a similar fashion as discussed for the single ratcheted channel. The position and size of the vortexes, and therefore the periodicity of the associated oscillatory motion will be controlled only by the geometrical parameters of the microchannel. This is in contrast to the vortex location originated from the Rayleigh–Bénard convection which is in principle undetermined, and also in contrast to their size which depends mostly on non-geometrical factors like the temperature gradient and the fluid viscosity.⁵⁶

Gear with circular confinement: Couette-like flow

All the previously proposed structures correspond to flat configurations, which are typical in the microchannels of lab-on-a-chip devices, but the principles explained here can be extended

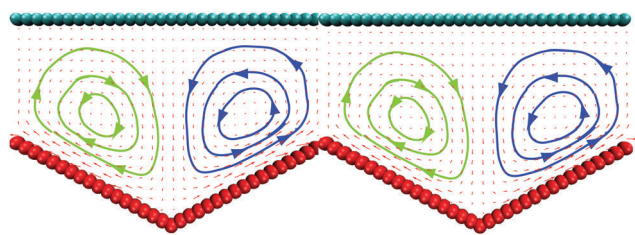


Fig. 5 Flow field and streamlines generated by a microchannel with a single symmetric ratcheted channel. Counter-rotating flow is highlighted with a different colored streamline.

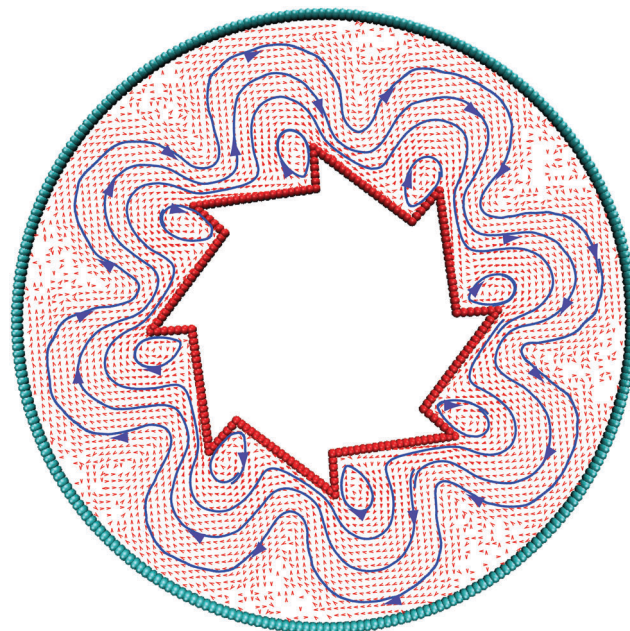


Fig. 6 Flow field and streamlines generated by a fixed gear confined in a circular wall. The flower-like structure of the flow proves the existence of an important traversing flow which globally stirs the fluid.

as well to circular geometries. This is the case of an asymmetrically ratcheted gear fixed and confined in the center of a circular wall. This would in fact be the fixed counterpart of the rotating gear that we investigated in our previous work.²³ The simulated flow field and the corresponding streamlines are displayed in Fig. 6, which are qualitatively similar to those of the single ratcheted flow in Fig. 1c. The resulting flow velocity could be approximated in the same way as determined for the single ratcheted channel, and we can in fact expect that to a good extent the dependence established in eqn (6) is also valid in this closed loop geometry. This means that a steering flow in the cylindrical direction is induced. Other closed geometries like those with two confronted or specularly oriented ratcheted walls will also be qualitatively similar to their straight counterparts. Note that the analytical calculation performed for a similar geometry based on the diffusioosmotic phenomenon^{26,27} assumes that the phoretic force is fixed per unit of the wall area. This predicts more significant recirculating streamlines, and much less pronounced traversing streamlines than the ones obtained in our study, which is associated with significantly smaller fluxes. Our simulation setup naturally takes into account a non-constant heat flux close to the surfaces arising from the temperature distribution as given by the geometrical constraints.

IV. Discussion and conclusion

Various microfluidic devices driven by external temperature gradients are here proposed based on channels with sawtooth profiled walls. The temperature gradient along the tooth edges drives a thermoosmotic fluid flow in the vicinity of the walls. By performing mesoscale hydrodynamic simulations using a

well-contrasted method, we probe several channel geometries. The flow direction and its intensity are determined by the thermophoretic properties of the wall–fluid interactions, as well as by the system dimensions, geometry, liquid viscosity and applied temperature difference. A single ratcheted channel is shown to pump fluids producing shear-like velocity profiles, while a double ratcheted channel is shown to pump fluids with an inverted capillary-like velocity profile. A specularly asymmetrically ratcheted channel is shown to display an elongational-type velocity profile, and a symmetrically ratcheted channel shows counter-rotating flows as those typical in Rayleigh–Bénard convection. Channels are not restricted to have a flat straight geometry, but circular or cylindrical geometries are also functional. In contrast with existing devices, the ones proposed here do not rely on any movable part, the presence of gravity or any externally imposed inlet or outlet flows, but only on the device properties and the external temperature differences.

The applied temperature differences can be experimentally achieved, for example, by laser illumination when one of the wall surfaces is metal coated.^{14,25} Manipulation with laser light brings two very significant advantages. One is that it provides a very precise time and space control of the temperature and consequently of the induced fluid flows. In cases where flow is necessary in only one part of a lab-on-a-chip device or only for some time or with certain periodicity, precisely controlled laser illumination would be beneficial. The second remarkable advantage is the improved portability and flexibility of light-driven fluidic chips which do not have to be physically connected to complex external electric or hydraulic devices.¹⁹ On the other hand, although in principle only single-component fluids are required, the presence of multiphase fluids will have similar, or eventually larger effects. Besides the geometry, large versatility of these devices is expected due to the high sensitivity of the wall–fluid thermophoretic properties which can vary with a large number of factors like average temperature, density and the fluid composition. As an alternative to laser illumination, temperature differences can also be achieved by having each microchannel wall in contact with heat reservoirs at different temperatures.^{57,58} This contact heating can be a practical construction in some cases, and can eventually benefit from existing residual temperature differences, which would allow these device to harvest part of waste heat, transforming it into flow motion. Similarly, and besides recovering the otherwise wasted heat, the device can facilitate the cooling down of microscale heat sources, such as microelectronic chips.

In order to demonstrate the pumping capability of the proposed microfluidic device under experimental conditions, we first estimate the relevant dimensionless numbers, such as the Peclet number $Pe = \nu L/D$. The diffusion coefficient D can be obtained from the Schmidt number Sc and the viscosity η given in the Model section. Employing then the characteristic values of the fluid velocity ν and the channel width, we obtain $Pe \simeq 1$. A different approach is to map the units of the mesoscale simulation model to those of real physical systems. Unfortunately, there are more than one mapping strategies, but here we choose a simple one which consists in directly equating the

dimension of the simulation channel to a microscale size. As an example, we consider the channel width $W = 10 \mu\text{m}$, which translates into the wall-bead radius to be $\sigma \simeq 0.6 \mu\text{m}$. Thus, the related bead mass can be calculated as $M = (4\pi/3)\sigma^3 d \simeq 9 \times 10^{-16} \text{ kg}$, by considering $d = 10^3 \text{ kg m}^{-3}$, the density of water. The fluid particle mass is taken in our simulation model to be $m = M$, such that we can map the velocity simulation units to real units $\sqrt{k_B \tilde{T}/m} \simeq 2 \times 10^3 \mu\text{m s}^{-1}$, with $\tilde{T} \simeq 300 \text{ K}$ being the ambient temperature. This rough estimation would allow us to translate the velocities in Fig. 1d, 2b, f, 3b and 4b, to be of about $1\text{--}10 \mu\text{m s}^{-1}$. Furthermore, this mapping also allows us to calculate other derived quantities such as the related shear rates $\sim 1 \text{ s}^{-1}$ and the employed temperature gradients of $5 \text{ K } \mu\text{m}^{-1}$ which are comparable to those employed in experiments with Au–silica Janus particles of $1 \text{ K } \mu\text{m}^{-1}$.¹⁴

Note that the above procedure cannot simultaneously map all the relevant physical quantities of the simulation system to reasonable real values, due to the mesoscale character of the simulation method. In this way, the solvent shear viscosity mapped using the above procedure corresponds to $\eta \simeq 7 \times 10^{-5} \text{ kg ms}^{-1}$, which is 14 times lower than that of water at room temperature, $10^{-3} \text{ kg ms}^{-1}$. Moreover, the dimensionless thermal diffusion factor of our wall beads, $\alpha_T \sim 6$, is much smaller than that of their experimental counterparts, like a carboxyl-modified polystyrene bead of $0.6 \mu\text{m}$ radius that measures a Soret coefficient of $S_T \simeq 10 \text{ K}^{-1}$,⁵⁹ corresponding to a thermal diffusion factor of $\alpha_T = S_T \tilde{T} \simeq 3000$. On the other hand, the flow velocity is determined by the ratio of α_T to η , as can be seen from eqn (2). The ratio obtained by mapping therefore underestimates its real value by a factor ~ 0.025 . Considering this factor, the flow velocity in a real microchannel can be estimated to be in the range $40\text{--}400 \mu\text{m s}^{-1}$, which is certainly strong enough to be employed in microfluidic applications.²

The above mappings provide us a very valuable estimate of the related orders of magnitude in real units. Most of the choices made in our simulations are biased by computational efficiency arguments, and not related to limitations of the physical phenomenon. In this way, simulations using larger systems, smaller temperature gradients, and larger values of the thermal diffusion factor α_T are in principle possible, and would provide considerably larger values of the Peclet number Pe and a much better matching to real systems, although they are unfortunately not straightforward at this stage. Interestingly, the experimental results of a self-thermocapillary asymmetrically ratcheted gear²⁵ show that the gear with an outer radius of $8 \mu\text{m}$ can rotate with a maximum angular velocity of 30 rad s^{-1} . This velocity value nicely agrees with our estimation, but would correspond to a much smaller temperature gradient and larger thermal diffusion factor than those employed in these simulations. Most importantly, the experimental results in ref. 25 constitute a strong argument in support of the feasibility of our approach.

In conclusion, devices based on thermoosmosis with asymmetrically ratcheted confining walls can therefore be realistically employed to manipulate multiple types of complex fluids,

and be the basis of different machines, such as a new generation of shear and extensional rheometers without any movable parts, stirrers, and various types of pumps, and promisingly devices able to recover waste heat or to facilitate cooling of microchips. Furthermore, this work is based on concepts of thermophoresis which have proved to apply to other phoretic effects in different structures. This is the case of catalytic microswimmers,^{60,61} and other diffusiophoretic machines.^{24,62} Therefore, extension of the conclusions presented here to other phoretically osmotic effects such as diffusioosmosis is to be expected.⁶³

Acknowledgements

We thank M. Pavlik Lettinga, Simone Wiegand, and Ke Chen for useful discussions. M. Y. gratefully acknowledges support from the National Natural Science Foundation of China (Grant No. 11674365 and 11404379). M. R. gratefully acknowledges financial support by the Deutsche Forschungsgemeinschaft via SPP 1726 Microswimmers. EU-COST action MP1305 "Flowing Matter" is kindly acknowledged. European patent application 14719222.3-1610 and German patent application 112014002171.7 are pending for this work.

References

- G. M. Whitesides, *Nature*, 2006, **442**, 368.
- T. M. Squires and S. R. Quake, *Rev. Mod. Phys.*, 2005, **77**, 977.
- H. Stone, A. Stroock and A. Ajdari, *Annu. Rev. Fluid Mech.*, 2004, **36**, 381.
- A. A. Darhuber and S. M. Troian, *Annu. Rev. Fluid Mech.*, 2005, **37**, 425.
- S. Gueron and K. Levit-Gurevich, *Proc. Natl. Acad. Sci. U. S. A.*, 1999, **96**, 12240.
- J. Elgeti and G. Gompper, *Proc. Natl. Acad. Sci. U. S. A.*, 2013, **110**, 4470.
- J. McGrath, S. Somlo, S. Makova, X. Tian and M. Brueckner, *Cell*, 2002, **114**, 61.
- C. Brennen and H. Winet, *Annu. Rev. Fluid Mech.*, 1977, **9**, 339.
- F. Fahrni, M. W. J. Prins and L. J. van IJzendoorn, *Lab Chip*, 2009, **9**, 3413.
- A. Babataheri, M. Roper, M. Fermigier and O. du roure, *J. Fluid Mech.*, 2011, **678**, 5.
- J. L. Anderson, *Annu. Rev. Fluid Mech.*, 1989, **21**, 61.
- A. Ajdari and J. Prost, *Proc. Natl. Acad. Sci. U. S. A.*, 1991, **88**, 4468.
- J. M. Catchmark, S. Subramanian and A. Sen, *Small*, 2005, **1**, 202.
- H. R. Jiang, N. Yoshinaga and M. Sano, *Phys. Rev. Lett.*, 2010, **105**, 268302.
- J. Palacci, B. Abécassis, C. Cottin-Bizonne, C. Ybert and L. Bocquet, *Phys. Rev. Lett.*, 2010, **104**, 138302.
- A. Siria, P. Poncharal, A.-L. Biance, R. Fulcrand, X. Blase, S. T. Purcell and L. Bocquet, *Nature*, 2013, **494**, 455.
- J. A. Cohen and R. Golestanian, *Phys. Rev. Lett.*, 2014, **112**, 068302.
- D. Psaltis, S. R. Quake and C. Yang, *Nature*, 2006, **442**, 381.
- D. Baigl, *Lab Chip*, 2012, **12**, 3637.
- C. Liu and Z. Li, *Phys. Rev. Lett.*, 2010, **105**, 174501.
- M. Yang and M. Ripoll, *Soft Matter*, 2013, **9**, 4661.
- A. D. Stroock, R. F. Ismagilov, H. A. Stone and G. M. Whitesides, *Langmuir*, 2003, **19**, 4358.
- M. Yang and M. Ripoll, *Soft Matter*, 2014, **10**, 1006.
- M. Yang, M. Ripoll and K. Chen, *J. Chem. Phys.*, 2015, **142**, 054902.
- C. Maggi, F. Saglimbeni, M. Dipalo, F. D. Angelis and R. Di Leonardo, *Nat. Commun.*, 2015, **6**, 7885.
- S. Michelin, T. D. Montenegro-Johnson, G. De Canio, N. Lobato-Dauziera and E. Lauga, *Soft Matter*, 2015, **11**, 5804.
- S. Michelin and E. Lauga, *Phys. Fluids*, 2015, **27**, 111701.
- R. Piazza and A. Parola, *J. Phys.: Condens. Matter*, 2008, **20**, 153102.
- A. Würger, *Rep. Prog. Phys.*, 2010, **73**, 126601.
- M. Yang and M. Ripoll, *J. Phys.: Condens. Matter*, 2012, **24**, 195101.
- S. Wiegand, *J. Phys.: Condens. Matter*, 2004, **16**, R357.
- A. Koeniger, N. Plack, W. Koehler, M. Siebenbuerger and M. Ballauff, *Soft Matter*, 2013, **9**, 1418.
- K. I. Morozov and W. Koehler, *Langmuir*, 2014, **30**, 6571.
- B. V. Derjaguin, N. V. Churaev and V. M. Muller, *Surface forces*, Consultants Bureau, New York, 1987.
- F. M. Weinert and D. Braun, *Phys. Rev. Lett.*, 2008, **101**, 168301.
- R. Di Leonardo, F. Ianni and G. Ruocco, *Langmuir*, 2009, **25**, 4247.
- A. Malevanets and R. Kapral, *J. Chem. Phys.*, 1999, **110**, 8605.
- M. Ripoll, K. Mussawisade, R. G. Winkler and G. Gompper, *Phys. Rev. E: Stat., Nonlinear, Soft Matter Phys.*, 2005, **72**, 016701.
- J. T. Padding and A. A. Louis, *Phys. Rev. E: Stat., Nonlinear, Soft Matter Phys.*, 2006, **74**, 031402.
- R. Kapral, *Adv. Chem. Phys.*, 2008, **140**, 89.
- M. Yang, M. Theers, J. Hu, G. Gompper, R. G. Winkler and M. Ripoll, *Phys. Rev. E: Stat., Nonlinear, Soft Matter Phys.*, 2015, **92**, 013301.
- J. F. Ryder, PhD thesis, University of Oxford, United Kingdom, 2005.
- G. Gompper, T. Ihle, D. M. Kroll and R. G. Winkler, *Adv. Polym. Sci.*, 2009, **221**, 1.
- E. Tüzel, T. Ihle and D. M. Kroll, *Phys. Rev. E: Stat., Nonlinear, Soft Matter Phys.*, 2006, **74**, 056702.
- G. A. Vliegenthart, J. F. M. Lodge and H. N. W. Lekkerkerker, *Physica A*, 1999, **263**, 378.
- D. Lüsebrink, M. Yang and M. Ripoll, *J. Phys.: Condens. Matter*, 2012, **24**, 284132.
- H. C. Andersen, *J. Chem. Phys.*, 1980, **72**, 2384.
- D. Lüsebrink and M. Ripoll, *J. Chem. Phys.*, 2012, **136**, 084106.
- M. Yang, A. Wysocki and M. Ripoll, *Soft Matter*, 2014, **10**, 6208.

- 50 T. Ihle, E. Tüzel and D. M. Kroll, *Europhys. Lett.*, 2006, **76**, 664.
- 51 N. Kikuchi, J. F. Ryder, C. M. Pooley and J. M. Yeomans, *Phys. Rev. E: Stat., Nonlinear, Soft Matter Phys.*, 2005, **71**, 061804.
- 52 A. Würger, *Phys. Rev. Lett.*, 2011, **107**, 164502.
- 53 A. A. Donkov, S. Tiwari, T. Liang, S. Hardt, A. Klar and W. Ye, *Phys. Rev. E: Stat., Nonlinear, Soft Matter Phys.*, 2011, **84**, 016304.
- 54 S. Hardt, S. Tiwari and T. Baier, *Phys. Rev. E: Stat., Nonlinear, Soft Matter Phys.*, 2013, **87**, 063015.
- 55 A. Groisman and S. R. Quake, *Phys. Rev. Lett.*, 2004, **92**, 094501.
- 56 M. C. Cross and P. C. Hohenberg, *Rev. Mod. Phys.*, 1993, **65**, 851.
- 57 F. M. Weinert, J. A. Kraus, T. Franosch and D. Braun, *Phys. Rev. Lett.*, 2008, **100**, 164501.
- 58 D. Vigolo, R. Rusconi, H. A. Stone and R. Piazza, *Soft Matter*, 2010, **6**, 3489.
- 59 S. Duhr and D. Braun, *Phys. Rev. Lett.*, 2006, **96**, 168301.
- 60 W. F. Paxton, K. C. Kistler, C. C. Olmeda, A. Sen, S. K. St. Angelo, Y. Cao, T. E. Mallouk, P. E. Lammert and V. H. Crespi, *J. Am. Chem. Soc.*, 2004, **126**, 13424.
- 61 L. F. Valadares, Y.-G. Tao, N. S. Zacharia, V. Kitaev, F. Galembeck, R. Kapral and G. A. Ozin, *Small*, 2010, **6**, 565.
- 62 M. Yang, R. Liu, M. Ripoll and K. Chen, *Lab Chip*, 2015, **15**, 3912.
- 63 M. Shen, F. Ye, R. Liu, K. Chen, M. Yang and M. Ripoll, *J. Chem. Phys.*, 2016, in press.